Proceedings of the ASME 2013 International Design Engineering Technical Conferences & Computers and Information in Engineering Conference
IDETC/CIE 2013
August 4-7, 2013, Portland, OR, USA

DETC2013-13038

MEMS BASED XY STAGE WITH LARGE DISPLACEMENT

Mohammad Olfatnia*, Leqing Cui, Pankaj Chopra, and Shorya Awtar
Precision Systems Design Laboratory, Mechanical Engineering
University of Michigan, Ann Arbor, MI 48109, USA

ABSTRACT

This paper presents a micro XY stage that employs electrostatic comb-drive actuators and achieves a bi-directional displacement range greater than 225 µm per motion axis. The proposed XY stage design comprises four rigid stages (ground, motion stage, and two intermediate stages) interconnected via flexure modules. The motion stage, which has two translational degrees of freedom, is connected to two independent single degree of freedom intermediate stages via respective parallelogram (P) transmission flexures. The intermediate stages are connected to the ground via respective Clamped paired Double Parallelogram (C-DP-DP) guidance flexures. The C-DP-DP flexure, unlike conventional flexures such as the paired Double Parallelogram flexure (DP-DP), provides high bearing direction stiffness (K_b) while maintaining low motion direction stiffness (K_m) over a large range of motion direction displacement. This helps delay the onset of sideways instability in the comb-drive actuators that are integrated with the intermediate stages, thereby offering significantly greater actuation stroke compared to existing designs. The presented work includes closed-form stiffness analysis of the proposed micro XY stage, finite elements simulation, and experimental measurements of its static and dynamic behavior.

1. INTRODUCTION AND BACKGROUND

Micro XY motion stages that allow large ranges of motion (≥ 100 µm) are desirable in several applications such as probe-based data-storage systems [1-3], scanning probe microscopy [4], and optical sensing and communication systems [5]. One limitation of the existing micro XY stages is their relatively small range of motion. Although large range single-axis micro stages have been reported [6], large range micro XY stages are rare in the current literature.

Various actuation schemes, mainly piezoelectric, electromagnetic, electrothermal and electrostatic [7], have been implemented in the micro XY stages reported so far. Electromagnetic actuation is common because of its linear current versus displacement curve and its relatively low actuation voltage. However, design and fabrication of a MEMS electromagnetic actuator with sufficient magnetic material mass and coil turns, capable of generating sufficient force, is difficult. Hybrid integration, i.e., assembling conventional electromagnetic actuators with a micro-fabricated MEMS device, has been generally used to overcome this problem [8]; for instance, see the IBM Millipede data-storage system with a stroke of 120 µm [1].

Electrothermal actuators are easily fabricated from a single material, and generally employ two connected arms with different cross sections to obtain differential thermal expansion. This differential thermal expansion provides a strong actuation force but a small deflection [9]. One may achieve large displacement thermal actuators by employing a very large beam length. For instance, Syms [10] reported a displacement of 500 µm at the resonant condition using an electrothermal actuator with a suspended beam length of 15 mm. This large footprint, along with its large thermal time constant, degrades the dynamic performance of these actuators; for instance, resonant frequency of this actuator was around 100 Hz. Moreover, the power dissipation and high working temperature (200º-600º C) are the other undesirable properties of thermal actuators [11].

Piezoelectric actuators consume considerably less amount of power and provide large mechanical forces and high resonant frequencies in a compact design; however, the primary limitation of these actuators is their inherently small stroke [12]. A relative expansion (or strain) of up to 0.2% is achievable with piezo stack actuators [13]. In an attempt to overcome the limited motion range in the above mentioned actuation schemes, actuators may be integrated with displacement amplifier mechanisms [14]. However, amplifying the motion range reduces the output force and bandwidth of the system, and increases the overall device footprint.

Electrostatic comb-drive microactuators are well established in the MEMS field because of their ease of fabrication. Comb-drive actuators provide high bandwidth and are operated using relatively high voltages [6]. The stroke of these actuators is generally limited by the sideways snap-in of the moving comb. We have recently showed that this early snap-in phenomenon can be avoided by carefully designing the guidance flexure of

* Corresponding Author (olfatnia@umich.edu, 734-730-3141)

Copyright © 2013 by ASME

the comb drive actuator. Strokes as high as 245 μm were achieved for 1 mm flexure beam length (L_l) and 6 μm comb gap (G) in a single direction at approximately 120 V [15]. This high stroke enables comb drive actuators to be implemented in applications that require large displacement. In this paper, we extend this single axis electrostatic actuator concept to a large range electrostatic XY micro stage. *Sections 2* and *3* present the design and analysis of the proposed XY stage. Finite element analysis results are presented in *Section 4* to simulate the vibration mode shapes of the device. *Section 5* summarizes the fabrication process and the experimental results demonstrating bi-directional displacement of 225 μm per axis in the XY stage.

2. XY STAGE DESIGN

2.1 Electrostatic comb drive actuators

A linear in-plane electrostatic comb-drive actuator comprises two electrically isolated conductive combs (fixed and moving) with N fingers each, schematically shown in *Figure 1*. The moving comb is guided via a flexure mechanism with relatively low stiffness (K_m) in the motion direction, and relatively high stiffness (K_b) in the bearing direction. When a voltage difference (V) is applied between the two combs, they experience an electrostatic attractive force, which displaces the moving comb by Y along the motion direction:

$$K_m \cdot Y = \frac{2\varepsilon_o H}{G} N V^2 \quad (1)$$

Here, ε_0 is the dielectric constant of air, G is the comb gap, and H is the out-of-plane thickness. The maximum displacement (stroke) is limited by the snap-in phenomenon, which corresponds to sideways instability of the moving comb [16]. For any Y displacement, the electrostatic force due to the actuation voltage V produces a destabilizing or negative spring effect and the flexure mechanism offers a stabilizing or positive spring effect in the X direction. The former increases while the latter generally decreases with increasing Y displacement. The Y displacement, at which the former stiffness exceeds the latter, the moving comb snaps sideways into the static comb. This condition determines the maximum actuation stroke of the actuator and may be mathematically expressed as [17]:

$$\left(\frac{K_b}{K_m}\right) \geq \frac{2Y^2}{G^2}\left(1+S\right) \quad (2)$$

The right hand side represents a "critical K_b/K_m stiffness ratio" needed to avoid snap-in, and clearly has to be large if a large actuation stroke is desired. Here, S is a positive margin of stability to account for the increase in the required K_b/K_m stiffness ratio when an error motion (E_x) is present. E_x includes any motion or misalignment of the moving comb in the X direction with respect to its nominal zero position due to flexure mechanics or fabrication imperfections, in the absence of electrostatic force. Clearly, to delay snap-in and maximize the actuator stroke, the flexure mechanism should provide a high (K_b/K_m) ratio over a large Y displacement range.

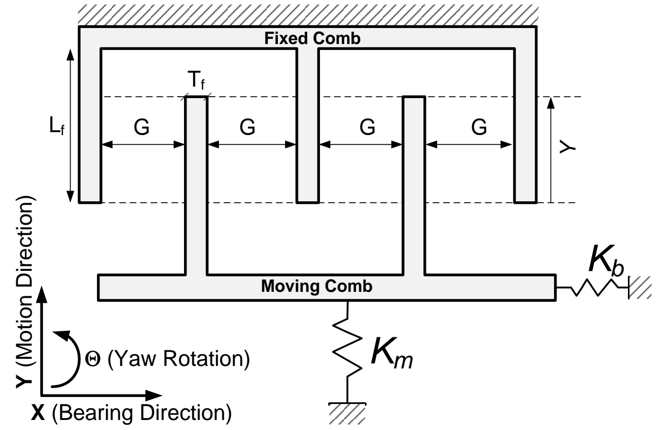

Figure 1: Schematic of an electrostatic comb drive with the springs representing the flexure bearing.

2.2 Serial vs. Parallel Kinematics

XY stages can be designed in serial-kinematic or parallel-kinematic configurations [18]. Both these configurations present unique challenges in meeting the large range motion objective. A serial kinematic XY stage is simply constructed by serially stacking one single-axis stage on the other. In fact, most macro-scale machines and metrology tools and many micro XY stages [19, 20] are built this way. This configuration leads to the actuator of the second axis being mounted on the motion stage of the first axis. This moving actuator and associated moving electrical connection present a challenge in MEMS fabrication and operation. Furthermore, this arrangement can cause the moving inertia load associated with the two axes and corresponding resonant frequencies of the axes to be different [21]. Except for applications that need a fast and slow axis such as scanning probe microscopy [22], such an attribute may not be desirable, in general. A parallel kinematic configuration, on the other hand, does not suffer from these drawbacks because of ground-mounted actuators. One of the most commonly implemented configurations for a comb-drive based micro XY stage employs a moving stage connected to the four surrounding identical comb drives via four sets of slender flexure beams [23, 24]. However, parallel-kinematic designs often suffer from cross-axis coupling errors as well as kinematic over-constraint, both of which lead to a restricted motion range.

2.3 Proposed Design Principle for XY micro stage

The configuration of the proposed XY micro stage is shown in *Figure 2*. There are four rigid stages: ground, motion stage, and two intermediate stages. The motion stage has two translational degrees of freedom with respect to ground. The intermediate stages are necessary to decouple the motion between the two axes and isolate the associated actuators from each other. The rigid stages in *Figure 2* are inter-connected by means of flexure modules that act as frictionless bearings and constrain relative motion. Each flexure module is a single degree of freedom mechanism that only allows translation in its

 Copyright © 2013 by ASME

respective motion direction and high stiffness in all other directions. The first intermediate stage is connected to ground by means of the first guidance flexure, which only allows relative motion along the X direction and constrains all the other degrees of freedom. This implies that irrespective of the rest of the mechanism, the first intermediate stage will have a primarily X displacement with respect to ground.

The first intermediate stage is connected to the motion stage by means of the first transmission flexure that allows for relative motion in the Y direction only and constrains all other relative motions. This implies that the X motion of the first intermediate stage will be largely transmitted to the motion stage, while any Y motion of the motion stage will not influence the first intermediate stage. Thus, the first intermediate stage becomes an ideal location for integrating the X actuator. The first guidance flexure provides a linear guide/bearing for the X actuator. Furthermore, any X force applied at the first intermediate stage produces minimal Y motion of the motion stage due to the presence of the first transmission flexure. In a similar manner, the same argument is true for the second guidance and transmission flexures and the second intermediate stage, which provides motion in the Y direction.

Ideally, in any deformed configuration of the flexural mechanism, the first intermediate stage always has an X displacement while the second intermediate stage has a Y displacement. The motion stage inherits the X displacement of first intermediate stage and the Y displacement of second intermediate stage, thus acquiring two translational degrees of freedom. Since all the connecting flexure units individually constrain rotation, the rotation of the motion stage is also constrained with respect to ground. This is an idealized scenario, where all guidance and transmission flexures are perfect single degree of freedom constraints. In reality, any flexure module will have only a finite compliance and range of motion along its degree of freedom (DOF), and a finite stiffness along its bearing or constraint directions. As a result, there will be finite error motions in the overall XY stage, the extent of which depends on the flexure modules that are chosen.

Furthermore, the electrostatic comb-drive actuator for each axis is placed between ground and the respective intermediate stage for that axis and the respective guidance flexure provides guidance between the fixed and moving combs of the actuator. The guidance flexures should offer high bearing direction stiffness (K_b) while maintaining low motion direction stiffness (K_m) over a large range of motion direction displacement, in order to mitigate the onset of sideways snap-in instability induced by the electrostatic actuation forces. These stiffness attributes in the guidance flexure help increase the actuation stroke along each axis in the proposed micro XY stage. A flexure module that is suitable for guidance of the intermediate stages is the Clamped Paired Double Parallelogram (C-DP-DP) flexure as shown in *Figure 2* and *Figure 3*, and introduced in our previous paper [15]. For transmission flexures, the main function is to transmit the motion from the intermediate stage to the motion stage with minimal motion loss and with the smallest possible mass and footprint. Moreover, the transmission flexure module in the X direction should provide minimal stiffness, i.e. resistance to motion, in the Y direction, and vice versa. The parallelogram (P) flexure satisfies these needs effectively with a small foot-print. To get the best motion performance at the motion stage, one needs to optimize the dimensions of C-DP-DP and P flexures along with the comb drive actuators. In the next section, these dimensions are chosen based on a closed form analysis [15, 25].

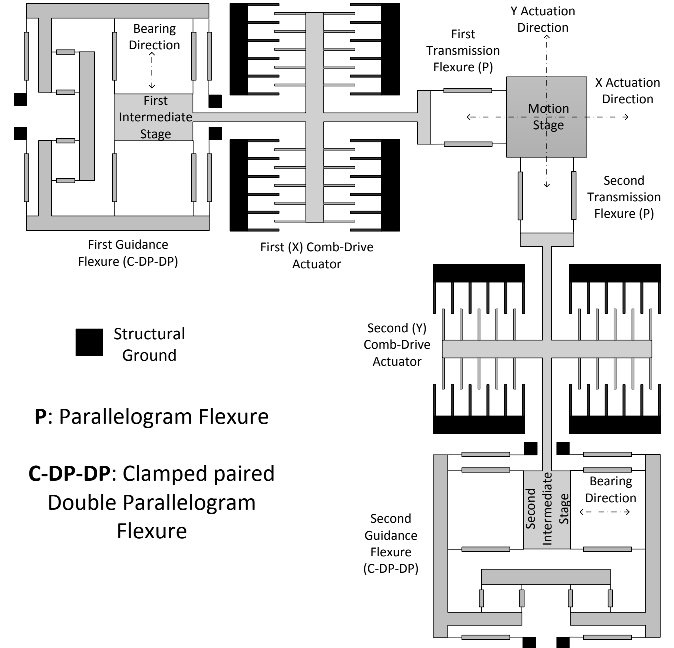

Figure 2: Proposed design of the comb drive based XY micro stage.

3. ANALYSIS

This section presents a closed form analysis of the key performance characteristics of the proposed micro XY stage, including stroke (Y_{max}), actuation effort (NV^2), first resonant frequency, and actuator error motion (δ). We define the latter as the undesired motion along bearing direction of one actuator due to the motion direction displacement of the other actuator.

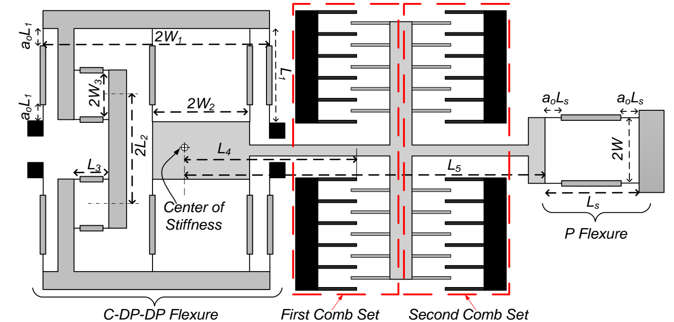

Figure 3: Detailed view of X actuator with two comb sets (H: device depth, T_1: beam thickness)

Copyright © 2013 by ASME

Note that there are two comb-sets per actuation axis to provide bi-directional actuation capability along each axis. The first comb-set in *Figure 3* provides actuation along the negative X axis, while the second comb-set provides actuation along the positive X axis.

3.1 Actuation Stroke and Effort

The analytical relations for the motion and bearing stiffness of the C-DP-DP and P flexures have been separately derived [26]. For the case of optimal clamp dimensions ($\left(W_3^2 L_1^3\right)/\left(2L_2^2 L_3 T_1^2\right)$*>100,)* the motion direction and bearing direction stiffness values for the C-DP-DP and P flexure are equal and are expressed in equation (3). The rotational stiffness of these two flexures are expressed in equation (4).

$$K_m = \frac{2EIk_{11}^{(0)}}{L^3}$$
$$K_b = \frac{2EI}{L^3}\frac{k_{33}}{\left(1+k_{33}g_{11}^{(1)}\left(\frac{Y}{2L}\right)^2\right)} \tag{3}$$

$$K_\theta\big|_{C-DP-DP} = \frac{2W_1^2W_2^2}{(W_1^2+W_2^2)}K_b; \qquad K_\theta\big|_P = W^2K_b \tag{4}$$

Here, E is the Young's modulus of the material and I is the second moment of area (= $HT_1^3/12$). All the dimensions that appear in these formulae are defined in *Figure 3*. The non-dimensional terms $k_{11}^{(0)}$, $k_{11}^{(1)}$, $g_{11}^{(1)}$, and k_{33} are all functions of the beam shape (a_o and T_1) and are referred to as beam characteristic coefficients [27]. These terms are mathematically expressed as follows:

$$k_{11}^{(0)} = \frac{6}{\left(3-6a_o+4a_o^2\right)a_o}$$
$$k_{11}^{(1)} = \frac{3\left(15-50a_o+60a_o^2-24a_o^3\right)}{5\left(3-6a_o+4a_o^2\right)^2}$$
$$g_{11}^{(1)} = \frac{2a_o^3\left(105-630a_o+1440a_o^2-1480a_o^3+576a_o^4\right)}{175\left(3-6a_o+4a_o^2\right)^3} \tag{5}$$
$$k_{33} = \frac{6}{a_0\left(T_1/L\right)^2}$$

Considering the equivalent mass-spring system of the proposed XY stage in any one direction, the motion direction stiffness is calculated as:

$$K_m = K_{m(C-DP-DP)} + K_{m(P)} = \frac{2EI_1}{L_1^3}k_{11}^{(0)} + \frac{2EI_s}{L_s^3}k_{11}^{(0)} = \frac{EHT_1^3}{6L_1^3}k_{11}^{(0)}\left(1+\left(\frac{L_1}{L_s}\right)^3\left(\frac{T_s}{T_1}\right)^3\right) \tag{6}$$

This equation is derived for a general case, where the beam length and thickness of the P flexure are different from C-DP-DP flexure and are L_s, and T_s, respectively. As mathematically expressed in equations (1) and (2), K_m should be minimized in order to achieve large stroke Y_{max}, and small actuation effort, NV^2. This implies that T_1 should be minimized. In fact, the value of T_1 is usually dictated by the practical limits of the micro-fabrication process. Furthermore, it can also be shown that in order to minimize K_m, T_s should be equal to T_1. Next, the effective bearing direction stiffness at each actuator comb-drive location (K_{bnet}) is given by:

$$K_{bnet} = \left(\frac{1}{K_b}+\frac{1}{\frac{K_\theta}{L_4^2}}\right)^{-1} \Rightarrow$$
$$K_{bnet} = K_b\left(\frac{2W_1^2W_2^2}{2W_1^2W_2^2+L_4^2(W_1^2+W_2^2)}\right) \tag{7}$$

where L_4 is the distance from Center of Stiffness (CoS) of the C-DP-DP flexure to the tips of the stationary comb fingers, for any given axis, as shown in *Figure 3*. CoS is the particular location in the C-DP-DP mechanism, where an applied bearing direction force results in zero rotation of the intermediate stage. The stroke of the micro XY stage is calculated by replacing K_{bnet} and K_m in equation (2):

$$Y_{max} = L_1\sqrt{\frac{2}{k_{33}g_{11}^{(1)}}\left(\sqrt{1+\left(\frac{G}{L_1}\right)^2\frac{\left(k_{33}\right)^2g_{11}^{(1)}\Phi}{2k_{11}^{(0)}\left(1+S\right)}}-1\right)}$$
$$where, \quad \Phi = \left(\frac{2W_1^2W_2^2}{2W_1^2W_2^2+L_4^2(W_1^2+W_2^2)}\right)\frac{1}{\left(1+\left(\frac{L_1}{L_s}\right)^3\right)} \tag{8}$$

In the Y_{max} relation, the second term in the second square root is typically two orders of magnitude larger than one. For instance, this value is $147 \gg 1$ with the dimensions listed in Table 1. Therefore, the Y_{max} relation can be further simplified to equation by assuming $L_1 = L_s$:

$$Y_{max} = L_1\sqrt{\frac{2}{k_{33}k_{11}^{(2)}}\left(\left(\frac{G}{L_1}\right)\left(k_{33}\right)\sqrt{\frac{k_{11}^{(2)}\Phi}{2k_{11}^{(0)}\left(1+S\right)}}-1\right)} \tag{9}$$

The actuation effort needed to achieve this stroke is found by substituting this displacement value in equation (1), as:

$$\frac{NV^2}{G} = \frac{k_{11}^{(0)}}{6}\left(\frac{E}{\epsilon_0}\right)\left(\frac{T_1}{L_1}\right)^3\left(1+\left(\frac{L_1}{L_s}\right)^3\right)Y_{max} \tag{10}$$

3.2 Actuator error motion in comb drive sets due to the cross-axis displacement of the motion stage

The transmission flexures connect the intermediate stages to the motion stage. Referring to *Figure 3*, ideally the X axis transmission flexure should provide a single translational DoF along the Y direction (i.e. zero compliance in this direction). This would ensure that a Y direction displacement of the motion stage does not produce any Y direction (i.e. bearing direction) error motions at the first intermediate stage and first guidance flexure. However, in practice, since the P transmission flexure has a finite compliance in the Y direction, the Y displacement of the motion stage does produce a small bearing direction displacement at the intermediate stage of the X

Copyright © 2013 by ASME

actuator. We refer to this undesired motion as the actuator error motion, which reflects a lack of perfect actuator isolation [12, 18]. This error motion in the comb drive sets introduces a destabilizing force, thus increasing the critical stiffness ratio in equation (2), and consequently reducing the $Y_{\max}$. In this section, a formulation for calculating this error motion at the comb derive sets, and its influence on the early snap-in of the comb sets is presented. Any Y displacement of the motion stage exerts a force at the first intermediate stage at the distance of L_5 from the CoS of the X direction C-DP-DP flexure, shown in *Figure 4*. The maximum value of this force ($F_{\max}$), which occurs when $Y = Y_{\max}$, is:

$$F_{\max} = \left(\frac{2EI_1}{L_s^3} k_{11}^{(0)} \right) Y_{\max} \tag{11}$$

This force and the resultant moment around the CoS tend to displace the comb fingers in the bearing direction from their nominal centered position. This displacement, which is greater for the second comb-set because of its geometric location, is given by:

$$\delta = \delta_{xy} + \delta_{xy\theta} = \left(\frac{F_{\max}}{K_b} + \frac{F_{\max} L_4 L_5}{K_\theta} \right) \Rightarrow$$
$$\delta = k_{11}^{(0)} Y_{\max} \left(\frac{1}{k_{33}} + g_{11}^{(1)} \left(\frac{Y_{\max}}{2L_1} \right)^2 \right) \left(\frac{L_1}{L_s} \right)^3 \left(1 + \frac{L_4 L_5 (W_1^2 + W_2^2)}{2W_1^2 W_2^2} \right) \tag{12}$$

This displacement appears as error motion ($E_x = \delta$) in equation (2), and therefore reduces the Y_{max}. This implies that, to accommodate this error motion, one has to employ a finite stability margin (S), which is mathematically given by equation (13) [15, 17]. For instance, with the current dimensions of the XY stage listed in table 1, the following estimates maybe obtained. Assuming $\delta = 0$ and therefore S=0, one can show that Y_{max} = 139 μm. However, for these actual XY dimensions, one can calculate δ = 0.12 μm, which corresponds to X_c = 1.06 μm, and S = 0.16. With this new value of required Stability Margin, the actuation stroke reduces to Y_{max}= 133 μm.

$$S = \left(1 + \frac{3X_c^2}{G^2} \right) \Bigg/ \left(1 - \frac{X_c^2}{G^2} \right)^2 - 1$$
$$\text{where} \qquad \delta = E_x = \frac{4X_c^3}{G^2 + 3X_c^2} \tag{13}$$

3.3 Resonant frequency

The resonant frequency of the stage is calculated by equation (14). This equation is derived using the Rayleigh's energy method, i.e., by equating the total maximum kinetic energy during the vibration cycle to the maximum potential energy [28].

$$f_{res} = \frac{1}{2\pi} \sqrt{\frac{K_m}{M}} = \frac{1}{2\pi} \sqrt{ \frac{ \frac{Ek_{11}^{(0)}}{6} \left(1 + \left(\frac{L_1}{L_s} \right)^3 \right) \left(\frac{T_1}{L_1} \right)^3 }{ \rho \left(A_p + \frac{1}{4} A_s \right) } } \tag{14}$$

In this equation A_p and A_s represent the area of parts moving at the velocity of the motion stage and half that velocity, respectively.

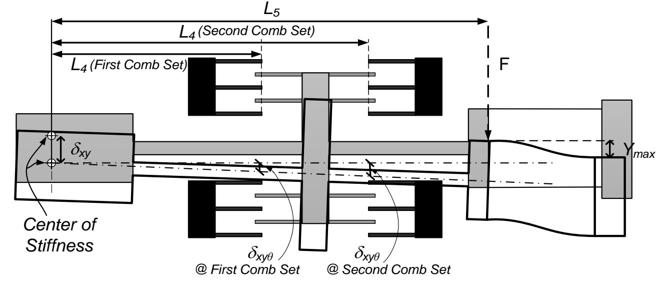

Figure 4: Displacement of the comb fingers due to $Y_{\max}$ at the motion stage. δ_{xy} is the displacement due to force $F_{\max}$, and $\delta_{xy\theta}$ is the displacement due to moment $M_{\max}$=$F_{\max}L_5$.

3.4 Design Summary

This section summarizes a step-by-step procedure to determine the various dimensions of the XY stage, including L_1, L_s, T_1, a_0, W_1, W_2, W, L_2, L_3, W_3, and G. The goal here is to maximize the actuation stroke while minimizing the device footprint and actuation voltage. A similar procedure to design large-stroke single-axis comb-drive actuators and associated guidance flexures was presented in detail in [15]; here, we extend that procedure to the proposed micro XY stage. The guidance and transmission flexures should offer high bearing direction stiffness (K_b) while maintaining low motion direction stiffness (K_m), over a large range of motion direction displacement. Without loss of generality, the design process starts with an assumed value of $L_1 = L_s$ = 1 mm for the length of flexure beams. The flexure beam thickness (T_1) is chosen to be a small value to lower the actuation effort and reduce the bending stress in the flexure beams. This value is dictated by the practical limits of the micro-fabrication process, T_1 = 3 μm. The beam shape $a_0 = 0.2$ is chosen to double the K_b / K_m for the same flexure beam thickness T_1. Comb-gap G = 6 μm is chosen to maximize stroke (larger than 100 μm per direction of each axis) while minimizing the actuation effort. Finally, W_1, W_2, L_2, L_3, W_3 and W are chosen such that rotational stiffness K_θ given by equation (4) and the clamp effectiveness parameter ($\left(W_3^2 L_1^3\right) / \left(2L_2^2 L_3 T_1^2\right)$) are adequately high to meet the assumptions of the above derivation and provide the desired stroke. All the dimensions of the stage are listed in Table 1.

Table 1: Dimensions of the XY Stages. All the dimensions are in micrometers (μm).

Flexure Design	G	T_f	N	L_f	T_1	L_1	L_2	L_3	L_4	L_5	L_s	W_1	W_2	W_3	H_1	a_0
C-DP-DP	6	4	140	175	3	1000	850	430	1385, 1550	2450	1000	775	250	240	50	0.2

Copyright © 2013 by ASME

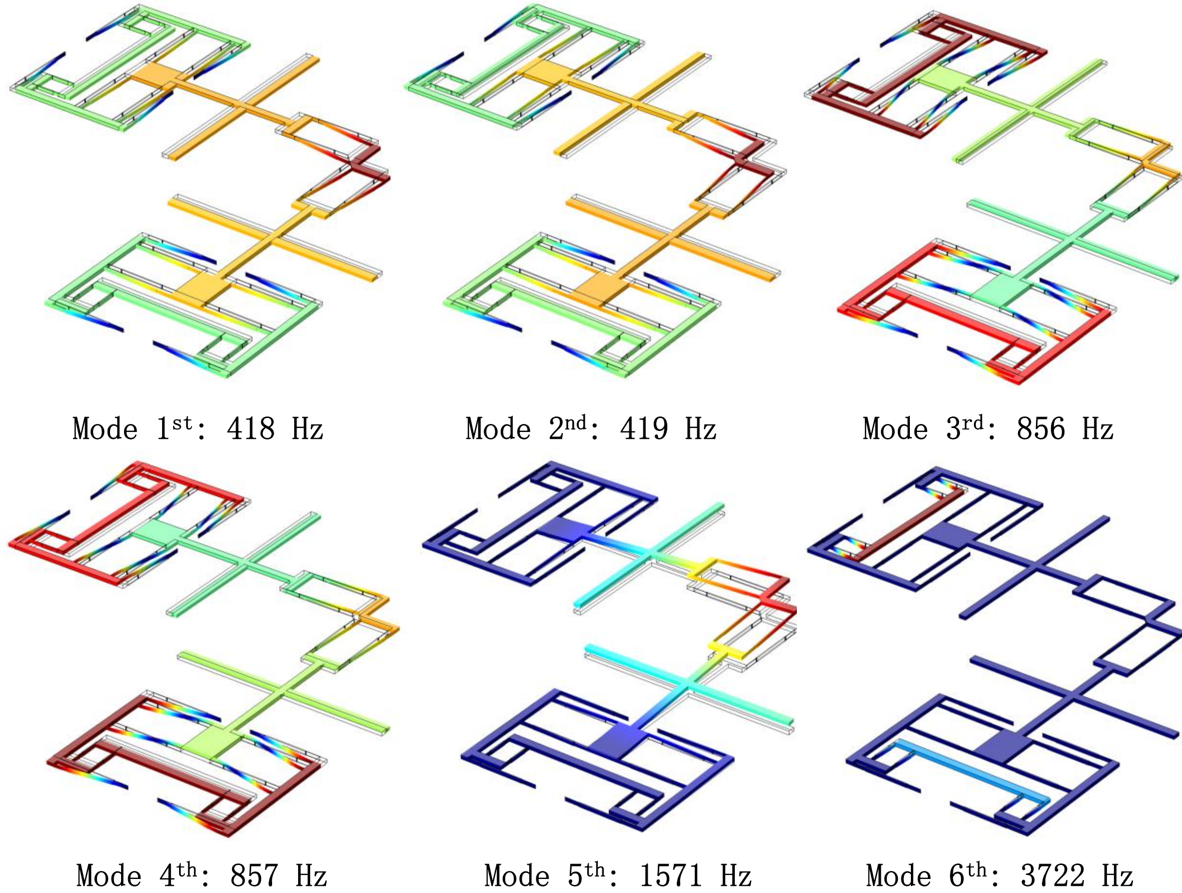

Figure 5: The first six mode shapes of the micro stage.

Table 2: Comb-drive XY stage resonant frequency and static displacement.

	L_4 *(μm)*	***First Resonant Frequency (Hz)***			***Predicted/Designed Stroke (μm)***		***Measured Stroke (μm)***	***Voltage at Stroke (V)***
		Theoretical	***FEA***	***Measured***	***S=0***	***S=1***		
First Comb Set	1385	414	418	400	139	115	124	94
Second Comb Set	1825				120	99	104	86

4. Mode shape analysis

In order to validate the theoretical analysis results of the previous sections and further evaluate the dynamic performance of the system under consideration, finite elements analysis (FEA) was conducted using the commercial software (COMSOL). Here, we specifically present the outcome of the modal analysis that was performed. The following material properties were used: density ρ = 2330 Kg/m^3, Young's modulus E = 164 GPa, and Poisson's ratio υ = 0.28. The first six mode shapes and their corresponding natural frequencies are shown in *Figure 5*.

The first and second mode shapes correspond to the translational vibration of the first intermediate stage, the second intermediate stage and the motion stage, and appear at around 418 Hz. The deformations of C-DP-DP and P flexures seen here validate the condition of used in estimating the first resonant frequency in equation (14). Compared to the theoretical result obtained in the previous section (414 Hz), the FEA result is approximately 1% lower.

Due to the symmetry along the diagonal direction of the motion stage, the 1st and 2nd modes, the 3rd and 4th modes, the 6th and 7th modes (latter not shown), etc., appear as pairs with their natural frequencies close to each other. The 3rd and 4th modes primarily involve the vibration of the secondary stages and the external clamp in both the C-DP-DP guidance flexures, while the two intermediate stages and the motion stage experience relatively little displacement. The 5th mode is an out-of-plane mode shape describing the vertical vibration of the intermediate stages and motion stage. This out-of-plane mode appears even before many in-plane modes, due to the smaller out-of-plane stiffness of the flexure modules compared to their in-plane stiffness. Finally, the 6th and 7th modes (latter not shown) are the in-plane vibration of the external clamp by itself in the C-DP-DP flexure modules.

Copyright © 2013 by ASME

5. Experimental Results and Discussion

5.1 Fabrication

The comb-drive actuators were fabricated using silicon on insulator (SOI) wafers with a device layer of 50 µm, a buried oxide layer of 2 µm, and a silicon handle layer of 350 µm. The device layer of the SOI wafers is heavily boron doped (P type) with resistivity less than 0.01 Ω.cm. The silicon device layer was first patterned and etched by deep reactive ion etching (DRIE), and then the silicon handle layer was patterned and etched by DRIE. Finally, buried oxide was removed by hydrofluoric (HF-49%) acid. After the last etching process, a critical point dryer was used to dry the samples to avoid stiction [29]. In this drying method, liquid CO_2 is transferred to vapor via the supercritical phase (@ T_c = 38°, P_c = 80atm) to avoid capillary forces that arise from the surface tension at the liquid–vapor interface. A scanning electron microscope (SEM) image of a representative fabricated device is shown in *Figure 6*.

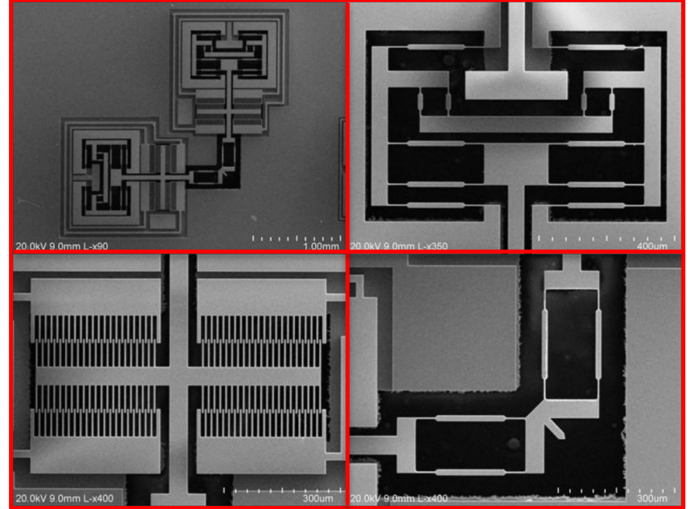

Figure 6: SEM image of a micro-fabricated XY stage.

5.2 Voltage-Stroke Curves

The fabricated comb-drive actuators were excited by applying DC voltages (Keithley 4200SCS) via connecting wires (Alessi probe station) to the fixed and moving combs. The voltage was swept in a ramp profile with 1 V increments from zero to a maximum of the actuator snap-in voltage. The displacement response of the actuators was observed with a microscope and captured by a CCD camera. Subsequently, the displacement of the actuators was quantitatively measured using image processing software. The motion direction displacement measurements were repeatable within 1 µm.

Figure 7 demonstrates the displacement versus voltage curves for the first and second comb sets of the X axis actuator in the micro XY stage. The measured stroke for the first and second comb set is 124 µm and 104 µm, respectively (Table 2). The measured strokes of the comb sets are different because the values of L_4 for the two comb sets are different. L_4 is the distance from the tip of comb finger to the CoS of the guidance flexure, as shown in *Figure 4*. L_4 is 1385 µm and 1550 µm for the first and second comb sets, respectively. A larger L_4 will reduce the effective bearing direction stiffness, as seen in equation (7), and consequently results in a smaller stroke. With a stability margin of S = 1, the theoretical stroke calculated from equation (8) for these two comb sets is 115 µm and 99 µm, respectively. The difference between the experimentally measured stroke and the theoretically calculated stroke corresponds to errors of 7% and 4%, indicating that S = 1 is a reasonable stability margin to be implemented in the theoretical prediction of actuation stroke.

Figure 7 presents a plot of the theoretical Y displacement versus actuation voltage. The theoretically predicted (equation (8)) and experimental results for these two cases agree within 22% and 17%, in the order that they are presented above. These discrepancies are within the expected range of deviation given the multiple sources of variability and uncertainty in dimensions and material properties in micro-fabricated devices.

To demonstrate that the fabricated XY stage is capable of simultaneous X and Y motion, a 180 µm by 180 µm square, shown in *Figure 8*, is scanned using the fabricated device. The motion range of the current device is compared to that of previously reported devices in the literature in *Figure 9*. It has previous shown that the maximum displacement of any flexure mechanism based single-axis comb drive actuator can be expressed as follows [15]:

$$Y_{\max} \propto \lambda \left(NV_{\max}^2\right)^{1/3} \left(L_1\right)^{4/3} \tag{15}$$

The first term on the right hand side of this equation (λ) depends on the stiffness and error motion characteristics of the flexure mechanism used. The second term represents actuation effort and device footprint (due to N), and should therefore be minimized. The third term represents the overall device footprint, and should also be minimized. Although the above expression is derived for single-axis electrostatic comb-drive actuators, we use it to compare XY electrostatic comb-drive actuators as well because the underlying physical relations remain the same. The horizontal axis in *Figure 9* is a representation of the actuation effort and the device footprint. The value of N is not included in this figure since it was not reported in many of the previously published papers. This figure shows the large motion range capability of the proposed micro XY stage design.

5.3 Resonant Frequency

The dynamic behavior (resonant frequency) of the stage is tested experimentally by implementing the "blur envelope" technique [28]. In this technique the resonant frequencies are determined by changing the frequency of an input drive signal of the form of ($V_{in}=V_p+V_d Sin(\omega t)$) until a blur envelope of the vibrating structure is observed. Since the excitation force depends on $(V_{in})^2$, the terms $V_pV_dSin(\omega t)$ and $(V_d)^2Cos(2\omega t)$ appear in the steady state response. To avoid the appearance of these two terms in the steady state response one can choose $V_p \gg V_d$ or $V_p \ll V_d$ based on the experimental conditions. It is

 Copyright © 2013 by ASME

worth mentioning that in the case of $V_p \ll V_d$, the frequency of the drive signal must be set to half that of the resonant frequency of the structure.

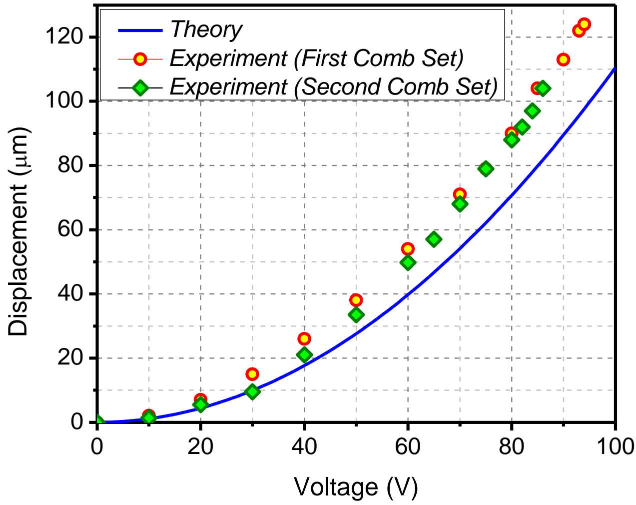

Figure 7: Y Displacement versus voltage for the first and second comb set of the micro stage.

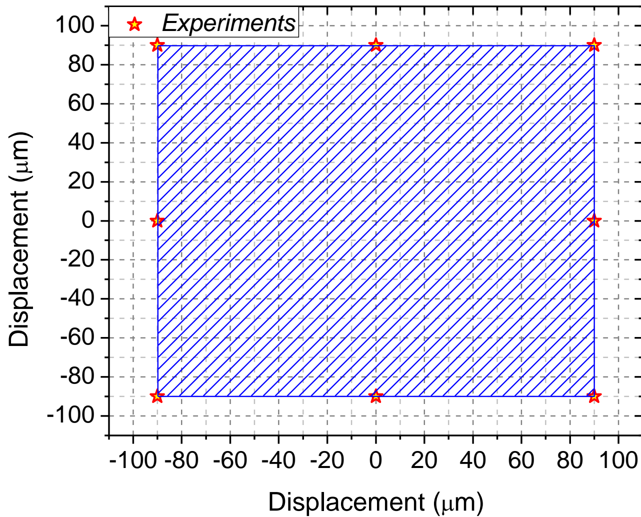

Figure 8: Simultaneous actuation of both X and Y axes to scan a 180 μm by 180 μm square.

In our experiments, a sinusoidal drive signal in the form of (*V = 3+50Sin(ωt)*) was generated by a signal generator (HP/Agilent 33220A) and amplified by a voltage amplifier (Avtek-110B). First, a frequency sweep was conducted to locate the device resonant frequency. Then, careful measurements were taken around that frequency to locate the exact value of the device's resonant frequency. The measured resonant frequency was 400 Hz, which is approximately 4% smaller than the theoretically and FEA predicted values, as shown in Table 2. The source of this discrepancy is most likely the dimensional variations in the micro-fabricated device.

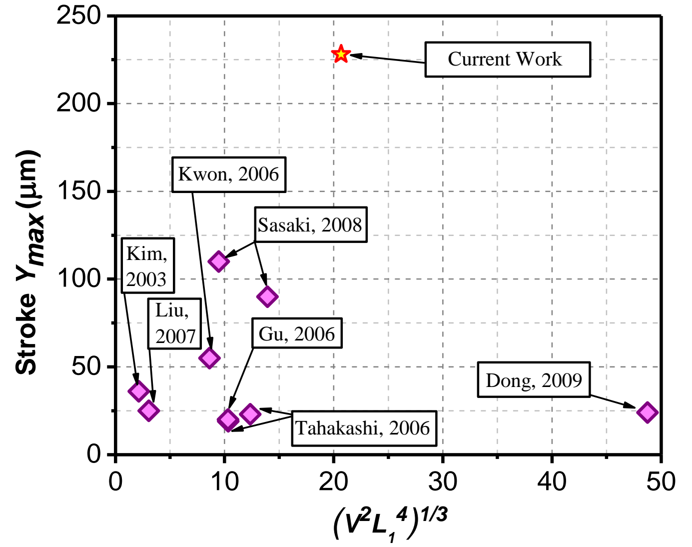

Figure 9: Comparison of the results of the tested micro stage in this paper with previously reported comb-drive XY stages (V and L_1 are in volts and mm, respectively.)

5. CONCLUSION

MEMS XY stages with a bi-directional displacement range greater than 225 μm per axis and a bandwidth of 400 Hz are reported in this paper. Possible applications include probe-based data-storage systems, scanning probe microscopy, and optical sensing and communication systems. The large range reported in this paper has been achieved by implementing the Clamped Paired Double Parallelogram (C-DP-DP) flexure as the guidance flexure and the Parallelogram (P) flexure as the transmission flexure in the X and Y directions.

ACKNOWLEDGEMENT

This research was supported, in part, by a National Science Foundation grant (CMMI # 0846738). The experimental portion of this work was performed at the Lurie Nanofabrication Facility, a member of the National Nanotechnology Infrastructure Network, which is also supported in part by the National Science Foundation.

REFERENCES

[1] E. Eleftheriou, T. Antonakopoulos, G. K. Binnig, G. Cherubini, M. Despont, A. Dholakia, U. Durig, M. A. Lantz, H. Pozidis, H. E. Rothuizen, and P. Vettiger, "Millipede - A MEMS-based scanning-probe data-storage system," *IEEE Transactions on Magnetics,* vol. 39, pp. 938-945, Mar 2003.

[2] M. Sasaki, F. Bono, and K. Hane, "Large-displacement Micro-XY-stage with paired moving plates," *Japanese Journal of Applied Physics,* vol. 47, pp. 3226-3231, Apr 2008.

[3] C. H. Kim, H. M. Jeong, J. U. Jeon, and Y. K. Kim, "Silicon micro XY-stage with a large area shuttle and no-etching holes for SPM-based data storage," *Journal of*

Copyright © 2013 by ASME

Microelectromechanical Systems, vol. 12, pp. 470-478, Aug 2003.
[4] J. Dong and P. M. Ferreira, "Electrostatically Actuated Cantilever With SOI-MEMS Parallel Kinematic XY Stage," *Journal of Microelectromechanical Systems,* vol. 18, pp. 641-651, Jun 2009.
[5] H. N. Kwon, J.-H. Lee, K. Takahashi, and H. Toshiyoshi, "MicroXY stages with spider-leg actuators for two-dimensional optical scanning," *Sensors and Actuators a-Physical,* vol. 130, pp. 468-477, Aug 14 2006.
[6] J. D. Grade, H. Jerman, and T. W. Kenny, "Design of large deflection electrostatic actuators," *Journal of Microelectromechanical Systems,* vol. 12, pp. 335-343, 2003.
[7] N. B. Hubbard, M. L. Culpepper, and L. L. Howell, "Actuators for micropositioners and nanopositioners," *Applied Mechanics Reviews,* vol. 59, pp. 324-334, 2006.
[8] S. Devasia, E. Eleftheriou, and S. O. R. Moheimani, "A survey of control issues in nanopositioning," *Ieee Transactions on Control Systems Technology,* vol. 15, pp. 802-823, Sep 2007.
[9] J. R. Reid, V. M. Bright, and J. H. Comtois, *Force measurements of polysilicon thermal micro-actuators* vol. 2882, 1996.
[10] R. R. A. Syms, "Long-travel electrothermally driven resonant cantilever microactuators," *Journal of Micromechanics and Microengineering,* vol. 12, pp. 211-218, May 2002.
[11] N. B. Hubbard and L. L. Howell, "Design and characterization of a dual-stage, thermally actuated nanopositioner," *Journal of Micromechanics and Microengineering,* vol. 15, pp. 1482-1493, Aug 2005.
[12] S. Awtar and G. Parmar, "Physical and control systems design challenges in large range nanopositioning," presented at the IFAC Symposium on Mechatronic Systems, Cambridge, MA, 2010.
[13] "Piezo Nano Positioning," P. Instrumente, Ed., ed, 2009.
[14] S. Kota, J. Hetrick, Z. Li, and L. Saggere, "Tailoring unconventional actuators using compliant transmissions: Design methods and applications," *IEEE-Asme Transactions on Mechatronics,* vol. 4, pp. 396-408, Dec 1999.
[15] M. Olfatnia, S. Sood, J. J. Gorman, and S. Awtar, "Large Stroke Electrostatic Comb Drive Actuators Enabled by a Novel Flexure Mechanism," *Journal of Microelectromechanical Systems,* 2013.
[16] R. Legtenberg, A. W. Groeneveld, and M. Elwenspoek, "Comb-drive actuators for large displacements," *Journal of Micromechanics and Microengineering,* vol. 6, pp. 320-329, 1996.
[17] S. Awtar and T. Trutna, "An Enhanced Stability Model for Electrostatic Comb-Drive Actuator Design," in *Proc. IDETC/CIE*, Montreal, Canada, 2010.
[18] S. Awtar, "Synthesis and Analysis of Parallel Kinematic XY Flexure Mechanisms," Ph.D., Massachusetts Institute of Technology, Boston, 2004.
[19] K. Takahashi, H. N. Kwon, K. Saruta, M. Mita, H. Fujita, and H. Toshiyoshi, "A two-dimensional f-theta micro optical lens scanner with electrostatic comb-drive XY-stage," *IECIE Electronics Express,* vol. 2, pp. 542-547, Nov 10 2005.
[20] K. Takahashi, M. Mita, H. Fujita, and H. Toshiyoshi, "A high fillfactor comb-driven XY -stage with topological layer switch architecture," *IECIE Electronics Express,* vol. 3, pp. 197-202, 2006.
[21] B. J. Kenton and K. K. Leang, "Design and Control of a Three-Axis Serial-Kinematic High-Bandwidth Nanopositioner," *Ieee-Asme Transactions on Mechatronics,* vol. 17, pp. 356-369, Apr 2012.
[22] T. Ando, "High-speed atomic force microscopy coming of age," *Nanotechnology,* vol. 23, Feb 12 2012.
[23] C. H. Kim and Y. K. Kim, "Micro XY-stage using silicon on a glass substrate," *Journal of Micromechanics and Microengineering,* vol. 12, pp. 103-107, Mar 2002.
[24] X. Liu, K. Kim, and Y. Sun, "A MEMS stage for 3-axis nanopositioning," *Journal of Micromechanics and Microengineering,* vol. 17, pp. 1796-1802, Sep 2007.
[25] S. Awtar, A. H. Slocum, and E. Sevincer, "Characteristics of beam-based flexure modules," *Journal of Mechanical Design,* vol. 129, pp. 625-639, Jun 2007.
[26] S. Sood and S. Awtar, "Clamped Symmetric Double Parallelogram Flexure Mechanism with Improved Bearing Performance," in *Review of Scientific Instruments*, ed.
[27] S. Awtar, K. Shimotsu, and S. Sen, "Elastic Averaging in Flexure Mechanisms: A Three-Beam Parallelogram Flexure Case Study," *Journal of Mechanisms and Robotics-Transactions of the Asme,* vol. 2, Nov 2010.
[28] W. C. Tang, "Electrostatic Comb Drive for Resonant Sensor and Actuator Applications," University of California, Berkeley, 1990.
[29] N. Tas, T. Sonnenberg, H. Jansen, R. Legtenberg, and M. Elwenspoek, "Stiction in surface micromachining," *Journal of Micromechanics and Microengineering,* vol. 6, pp. 385-397, Dec 1996.

 Copyright © 2013 by ASME